Inorganic Chemistry

Article

pubs.acs.org/IC

Activation Barriers of Oxygen Transformation at the Active Site of [FeFe] Hydrogenases

Arndt R. Finkelmann, Martin T. Stiebritz, and Markus Reiher*

Laboratorium für Physikalische Chemie, ETH Zürich, Valdimir-Prelog-Weg 2, 8093 Zürich, Switzerland

Supporting Information

ABSTRACT: Oxygen activation at the active sites of [FeFe] hydrogenases has been proposed to be the initial step of irreversible oxygen-induced inhibition of these enzymes. On the basis of a first theoretical study into the thermodynamics of O_2 activation [*Inorg. Chem.* **2009**, 48, 7127] we here investigate the kinetics of possible reaction paths at the distal iron atom of the active site by means of density functional theory. A sequence of steps is proposed to either form a reactive oxygen species (ROS) or fully reduce O_2 to water. In this reaction cascade, two branching points are identified where water formation directly competes with harmful oxygen activation reactions. The latter are water formation by O−O bond cleavage of a hydrogen peroxide-bound intermediate competing with H_2O_2 dissociation and CO_2 formation by a putative iron-oxo species competing with protonation of the iron-oxo species to form a hydroxyo ligand. Furthermore, we show that proton transfer to activated oxygen is fast and that proton supply to the active site is vital to prevent ROS dissociation. If sufficiently many reduction equivalents are available, oxygen activation reactions are accelerated, and oxygen reduction to water becomes possible.

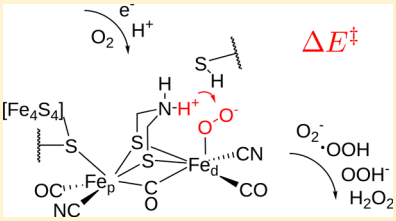

1. INTRODUCTION

The efficient catalysis of H_2 oxidation and formation is the outstanding feature of hydrogenase enzymes.[1] [FeFe], [NiFe], and [Fe] hydrogenases are the three classes of hydrogenases named according to the metal content of their active site.[2,3] Whereas [Fe] hydrogenase needs an additional substrate,[4] [NiFe] and [FeFe] hydrogenases catalyze the direct hydrogen oxidation or formation.[5] The catalytically more active [FeFe] hydrogenases[6] have a bias for H_2 formation, whereas [NiFe] hydrogenases have a bias for hydrogen oxidation.[7] These properties make [FeFe] hydrogenases the perfect candidates for biological fuel production.[8−10] The rapid and irreversible inhibition of [FeFe] hydrogenases by oxygen,[6,7,11−13] however, poses a severe constraint for technological applications.

Experimental[14,15] and theoretical[16] findings indicate that O_2-induced inhibition of [FeFe] hydrogenases is initiated by formation of a reactive oxygen species (ROS) at the active site, the so-called H cluster. To date almost no information on transition states and barrier heights has been published. We will close this gap in this work. The H cluster consists of a $[Fe_4S_4]$ cubane bound to a di-iron complex, called $[2Fe]_H$ subcluster, where the iron atom proximal to the cubane is labeled Fe_p and the iron atom distal to the cubane is Fe_d (see Figure 1 below).[17] Fe_d has a vacant coordination site where catalysis is believed to proceed.[18] This site must be important for the oxygen inhibition process as well since carbon monoxide, a fast and reversible inhibitor, binds to this site[19] and protects the enzyme against O_2-induced damage.[14,15,20] Theoretical investigations demonstrated that oxygen activation at this site is thermodynamically possible[16,21,22] and ROS formation can occur. Very recently, Kubas et al. determined O_2 binding to be exergonic by −7.1 kcal/mol with an activation free-energy barrier of +12.9 kcal/mol.[21]

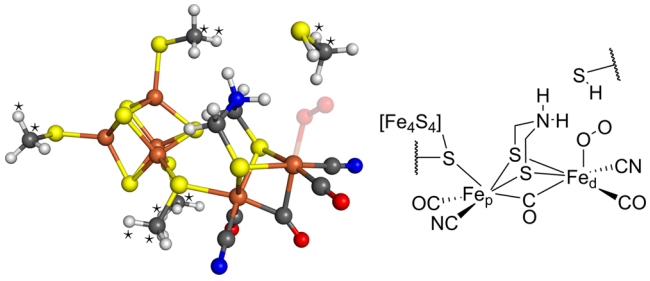

Figure 1. (left) Model structure of the [FeFe] hydrogenase active site with protonated bridgehead amine. Spatially fixed atoms are marked by a star. An oxygen molecule (transparent) is attached to the coordination site where catalysis proceeds. (right) Truncated structural representation of this active-site model employed in this work.

Furthermore, X-ray absorption spectroscopy combined with electrochemical measurements for the [FeFe] hydrogenase from *Chlamydomonas reinhardtii* revealed that the cubane is destroyed before the $[2Fe]_H$ subsite breaks down.[15] Thus, the current picture of O_2-induced inhibition of [FeFe] hydrogenases can be summarized as ROS formation at the $[2Fe]_H$ subsite followed by destruction of the $[Fe_4S_4]$ cubane by ROS.[14−16,23−25]

In contrast to [FeFe] hydrogenases, [NiFe] hydrogenases are generally not irreversibly inhibited by O_2.[26] Hence, a comparison to [NiFe] hydrogenases is instructive. Two types of oxygen insensitive or tolerant [NiFe] hydrogenases exist, which achieve oxygen insensitivity or tolerance by different strategies. The oxygen insensitivity of [NiFe] sensor hydrogenases (e.g., from *Ralstonia eutropha*[27]), which represents the first type, was

Received: May 7, 2014
Published: October 27, 2014

dx.doi.org/10.1021/ic501049z | *Inorg. Chem.* 2014, 53, 11890−11902

attributed to the narrowing of known gas diffusion channels.[28−30] Several studies addressed gas diffusion as a possibility to reduce O_2 sensitivity by mutagenesis experiments[31−34] and molecular dynamics (MD) simulations,[35−38] also for a [FeFe] hydrogenase.[39] However, complete oxygen tolerance or full catalytic activity over long time scales under aerobic conditions could not be realized yet.[10] Recent MD simulations suggest that shutting down the major diffusion pathways still not fully prevents O_2 diffusion to the active site.[37]

Certain [NiFe] hydrogenases from the bacteria *Ralstonia eutropha*, *Ralstonia metallidurans*, and *Hydrogenovibrio marinus*, which belong to the second type of O_2-tolerant enzymes, are reported to catalyze H_2 oxidation even under atmospheric conditions and at low H_2 concentration.[40,41] They feature a $[Fe_4S_3]$ iron−sulfur cluster coordinated by six instead of four cysteines.[42−44] The oxygen tolerance of these [NiFe] hydrogenases is attributed to the ability of this special FeS cluster to access three redox states within a narrow potential range.[45,46] It has been postulated that the additional reduction equivalents available, might help the enzymes to reduce O_2 to water, which prevents damage to the active site.[45−47]

It is therefore central to understand the nature of the active site of [FeFe] hydrogenases that does not allow for a full reduction of molecular oxygen to water. Aerobical as-isolated [FeFe] hydrogenases are in an electron paramagnetic resonance (EPR)-silent oxidized inactive state H_{ox}^{inact}. In this state, an oxygenic ligand (most probably OH^- or H_2O) is bound at the open coordination site at Fe_d[17] and the enzyme is air-insensitive. Early computational studies suggested a hydroxo ligand.[48] Upon one electron reduction, the enzyme enters the EPR-active transient state H_{trans} (presumably $[Fe_4S_4]^{1+}[Fe(II)Fe(II)]$).[49,50] The catalytically active oxidized state H_{ox} is formed by transfer of one electron from the cubane to the $[2Fe]_H$ subcluster with oxidation state $[Fe_4S_4]^{2+}[Fe(II)Fe(I)]$, which is presumably accompanied by a conformational change.[48−53] The H_{ox} state is O_2 sensitive[49−51,53] and rapidly inhibited by CO, which reversibly binds to Fe_d.[19,54−56] Because both species, H_{trans} and H_{ox}, are EPR detectable, either zero or two electrons are required in the transition from H_{trans} to H_{ox}.[49−51,55] Van Dijk et al. reported that reoxidation of H_{ox} into the H_{ox}^{inact} state is possible by two-electron oxidation[57] in the [FeFe] hydrogenase from *Desulfovibrio vulgaris* strain Hildenborough. An infrared spectroscopy study of the process suggested that the H cluster is not directly involved in this redox process.[55] Upon further reduction of H_{ox}, the active reduced state H_{red}, $[Fe_4S_4]^{2+}[Fe(I)Fe(I)]$ (EPR-silent) is accessed.[58]

The observations that the H_{ox}^{inact} state is air stable (vacant coordination site is occupied) and that the active site presumably reduces O_2 to a ROS but not fully to water are puzzling; especially in comparison to [NiFe] hydrogenases, which appear to achieve oxygen tolerance by oxygen reduction. On the basis of a first theoretical study on possible oxygen activation reactions at the active site of [FeFe] hydrogenase,[16] where we showed that O_2 activation is thermodynamically possible, we here present a detailed reaction scheme for various oxidation states including reaction barriers to elucidate the most likely reaction paths of oxygen at the $[2Fe]_H$ subcluster.

To describe the oxygen activation process, we assume that protons can be transferred to the active site and that the bridgehead amine group is the terminal part of the proton transfer relay to the H cluster. Such a concerted proton transfer from the protein exterior to the bridgehead amine group was observed in hybrid quantum mechanical/molecular mechanical simulations.[59,60] We will consider oxygen activation at the H cluster with and without simultaneous reduction steps and draw conclusions on competing oxygen degradation reactions.

2. COMPUTATIONAL METHODOLOGY

Our structural model of the active site includes the H cluster with dithioethylamine as bridging ligand[61] and the side chain of Cys299 (labeling according to PDB structure 3C8Y[62]). It is depicted in Figure 1. Apart from the bridgehead group, it is similar to the model of our previous study.[16] The model is derived from the crystal structure of the [FeFe] hydrogenase from *Clostridium pasteurianum* (PDB entry 3C8Y[62]). Bonds that were cut, when the model was extracted from the crystal structure, were saturated with hydrogen atoms. Their bond lengths were adjusted to the same length as in ref 24, and both atoms of the bond were kept fixed during structure optimization to preserve the structural constraints of the protein matrix (fixed atoms are indicated in Figure 1). Calculations were carried out with version 6.3.1 of the Turbomole program package.[63,64] The structures were optimized with the BP86-D3 density functional[65−67] approximation and single-point calculations on optimized structures were conducted with the COSMO model[68] ($\varepsilon = 4$), with a modified radius for iron (1.391 Å) as suggested in ref 69, to account for electrostatic screening. The def2-TZVP basis set[70] was chosen for all atoms (structure optimization and singlepoint calculations) and the resolution-of-the-identity (RI) approximation was invoked to speed up calculations.[71] To describe the antiferromagnetic coupling in the H cluster the broken-symmetry approach[72−75] was chosen. The antiferromagnetic coupling pattern in the cubane was adjusted as suggested in ref 76. (Both Fe atoms in the cubane proximal to Fe_p are antiferromagnetically coupled to the other two Fe atoms of the cubane and antiferromagnetically coupled to the $[2Fe]_H$ subsite, if it carries spin.) The methodology follows that of previous studies on [FeFe] hydrogenases in our and other laboratories.[16,24,77−79] The discussed local spins are expectation values of the local $\langle \hat{S}_{z,A} \rangle$ operator[80] and obtained by Mulliken population analysis[81] as implemented in Turbomole.[64] They are a measure for the difference in α and β electron density on an atom.

All species were calculated in the low-spin state (singlet or doublet) except of isolated oxygen, which was assumed to be in the triplet ground state before coordination. The spin crossover upon oxygen coordination might proceed by electron transfer from the H cluster to the O_2 molecule, as described in ref 21.

For each species we may assign the oxidation states of Fe_p and Fe_d and the charge state of the cubane (+3/ +2/ +1). To rationalize oxidation states, local spins on relevant atoms are discussed in the text. This is possible because Fe(II) centers feature no spin excess in the strong ligand environment of the $[2Fe]_H$ subsite. In combination with electron counting this allows us to qualitatively discriminate Fe(I) from Fe(III) for iron centers that feature local spin. Tables of local spins on every atom of every intermediate, as well as Cartesian coordinates, are given in the Supporting Information. For most intermediates there are multiple conformations possible (e.g., generated by orientation of the thiol S−H bond). A complete sampling of possible conformations is computationally not feasible, and we identified the most important conformations by chemical reasoning. For some reactions we were not able to optimize transition states but estimated the transition barriers by a potential energy surface (PES) scan. A PES scan is a stepwise optimization of structures between reactant and product. If, for example, atom A is transferred to atom B the distance A−B is varied in steps from the one in the reactant structure to the one in the product structure with relaxation of all other coordinates at each step. Note that all barriers of proton transfer reactions are classical barriers. Tunneling effects are not considered.

The accurate calculation of ligand dissociation free energies is difficult as accurate calculation of entropic contributions requires molecular-dynamics simulations, which is beyond the scope of this work considering the large number of reactions investigated. For isolated species in the gas phase, they may be estimated in the particle in the box, rigid rotor and harmonic oscillator approximations. Within our cluster approach it is, however, not possible to accurately calculate vibrational contributions, because atoms are fixed in space. Moreover, the translational

contribution for a particle in the box is worrisome for reactions in condensed phase that change the number of reactants as this yields a constant shift of about 10 kcal/mol per excess molecule.[82] In a recent study, Kubas et al.[21] estimated the entropic contribution of oxygen coordination to the H cluster to be 9.9 kcal/mol. These authors accounted for loss of translational entropy of the O_2 molecule due to penetration of the enzyme and a reduced available volume in the cavity,[21,36] zero-point energy and enthalpy changes. In the present study, the entropic contribution of ligand dissociation reactions is estimated by the rotational and translational contributions only. Note that for all other reactions electronic energy differences (ΔE_{el}) are reported, $\Delta E = \Delta E_{el}$. For the calculation of the translational partition function the volume of the protein cavity was chosen to be $V_{cavity} = 1.13 \times 10^{-28}$ m^3 to incorporate loss of translational energy due to diffusion through the protein, as suggested by Kubas et al.[21] The resulting entropy contributions at 298.15 K are $T\Delta S(O_2) = 11.0$ kcal/mol; $T\Delta S(O_2^-) = 11.1$ kcal/mol; $T\Delta S(O_2^{\bullet}) = 12.5$ kcal/mol; $T\Delta S(O_2^-) = 12.6$ kcal/mol; $T\Delta S(H_2O_2) = 12.9$ kcal/mol; $T\Delta S(H_2O) = 10.4$ kcal/mol; $T\Delta S(OH^{\bullet}) = 8.9$ kcal/mol; $T\Delta S(OH^-) = 8.9$ kcal/mol, where $T\Delta S = T(\Delta S_{trans} + \Delta S_{rot})$. Approximate ROS dissociation energies are then calculated as difference in electronic energy (including electrostatic embedding) between reactants and products plus gain in entropy of the dissociating ligand

$$\Delta E_{dissoc} = \Delta E_{el} - T(\Delta S_{trans} + \Delta S_{rot}) \quad (1)$$

Energies of ligand association reactions (ΔE_{assoc}) are calculated analogously.

These dissociation energies contain a contribution originating from dispersion interactions, which are a sum over atom-pairwise terms (D3 approximation[67]). In the ligand-bound reactants there are more pairwise interactions (dissociating ligand to remaining system) than in the products, because the products were calculated as separated and isolated systems. In the reactants, the pairwise interactions of the bound ligand to the remaining system are on the order of 7 kcal/mol for O_2, 8 kcal/mol for $HO_2^{\bullet}$ and HO_2^-, 6 kcal/mol for $HO^{\bullet}$ and HO^-, 11 kcal/mol for H_2O_2, and 8 kcal/mol for H_2O (lower for water bound via hydrogen bonding). These ligand-H cluster dispersion contributions energetically penalize ligand dissociation reactions. In the enzyme they are compensated in parts by new dispersion contacts of the dissociated ligand. Our model, however, does not account for the new dispersion contacts of the dissociated ligand. To estimate the effect of dispersion corrections on ligand dissociation reactions, we calculated the dissociation of H_2O_2 from $[Fe_4S_4]^{3+}[Fe(II)Fe(II)]^{NH/SH}-O_2H_2$ also without D3 (reoptimized structures, $\varepsilon = 4$). The reaction is endothermic by +3.6 kcal/mol without D3, instead of +12.9 kcal/mol with D3. Thus, incorporation of dispersion interactions, which is desired for a correct description of the active site, will lead to a less favorable ROS dissociation reaction (9.3 kcal/mol for H_2O_2) if such interactions cannot be properly modeled for the dissociated species (e.g., if the reference state is a dissociated isolated species that lacks dispersion interactions with the environment as the environment cannot be modeled properly).

Additional contributions to the solvation energy of the dissociated ligands arise from short-range nonelectrostatic solvation effects such as cavitation, dispersion, and solvent structural effects. We calculated these contributions with the *solvation model density* (SMD) approach of Marenich et al.[83] as implemented in Gaussian09.[84] The resulting energies are small (at most 1.5 kcal/mol for H_2O_2) and are therefore neglected in the presentation below. However, nonpolar contributions to the solvation energies for all ligands considered are given in the Supporting Information.

The calculation of the electronic energy difference is complicated further because the reference state of the products is not well-defined. I.e. for determining the reference state it must be assumed whether the dissociated species still is in a protein cavity with $\varepsilon \approx 4$ (cavity reference state, reaction energies denoted by $\Delta E^{(4)}$) or in bulk solvent in the final state with $\varepsilon \approx 80$ (solvated reference state, reaction energies denoted by $\Delta E^{(80)}$). This has a large influence on the dissociation energies of charged species and we thus calculated the electronic energy of the dissociated ligand always for the cavity reference state ($\varepsilon = 4$) and for the solvated reference state ($\varepsilon = 80$) of the dissociated ligand. Protonation energies were calculated by assuming an energy of −262.4 kcal/mol[85,86] for a solvated proton. Reduction energies were calculated as differences in electronic energy of the relaxed reactant and the one-electron reduced product structure. Note that, because of the charge of our H cluster model, protonation energies or coupled reduction/protonation energies are affected by charge recombination effects that are difficult to model in our approach. Relative energies for the same total charge state are, however, most accurate for the chemical interpretation of the data.

3. OXYGEN ACTIVATION WITHOUT EXTERNAL REDUCTION EQUIVALENTS

As a first scenario, a complete reduction of O_2, in the absence of external electron supply (electrons for O_2 reduction have to be provided by the H cluster's Fe atoms), is considered. The fast oxygen inhibition of different [FeFe] hydrogenases under H_2 oxidation conditions in electrochemical experiments,[14,20] where electrons are removed from the active site to the electrode, implies that external electron supply to the active site might not be crucial for oxygen activation at the H cluster. Scenarios with possible transfer of external electrons to the active site are investigated in later sections.

3.1. Oxygen Coordination to Fe_d and Subsequent Protonation. The first reaction steps are depicted in Figure 2. The oxygen activation process starts with coordination of triplet oxygen to Fe_d in the H_{ox} state, which is exothermic ($\Delta E^{(4)}_{assoc} = -12.3$ kcal/mol, $\Delta E^{(80)}_{assoc} = -12.2$ kcal/mol). Population analysis and the O_2 bond length of 1.321 Å, which is typical for a superoxide,[87,88] show that the oxygen coordination leads to oxidation of Fe_d and superoxide formation (see refs 16 and 24 for details). Superoxide dissociation is energetically slightly unfavored for the cavity reference state ($\Delta E^{(4)}_{dissoc} = +7.1$ kcal/mol) and energetically favored for the solvated reference state (dissociated ligand calculated with $\varepsilon = 80$, $\Delta E^{(80)}_{dissoc} = -18.1$ kcal/mol). Protonation of the bridgehead amine group, which is exothermic by −55.6 kcal/mol, leads to the stable species $[Fe_4S_4]^{2+}[Fe(II)\text{-}Fe(II)]^{NH_2^+/SH}-OO^-$ (compare Figure 2), where the bound oxygen species is still a superoxide (bond length of 1.334 Å, local spins of Fe_p and Fe_d are 0.0 a.u. and 0.25 a.u., respectively). Superoxide dissociation is less favored than from the unprotonated species ($\Delta E^{(4)}_{dissoc} = +24.6$ kcal/mol or $\Delta E^{(80)}_{dissoc} = -0.6$ kcal/mol).

Further activation of the bound O_2^- requires proton transfer to the O_2^- moiety, which could also trigger additional electron transfer to form peroxide. Our model contains two possible proton donors, the bridgehead ammonium group ($R_2N^BH_2^+$) and the thiol of Cys299. Proton transfer from the bridgehead $R_2N^BH_2^+$ moiety to the oxygen atom distal to Fe_d (O_d) leads to the hydrogen peroxide anion-bound species $[Fe_4S_4]^{2+}[Fe(II)\text{-}Fe(III)]^{NH/SH}-OOH^-$. This proton transfer is triggered by the rotation of the O_2 around the Fe−O_p bond (see Figure 1) toward the $R_2N^BH_2^+$ moiety and is exothermic by −3.4 kcal/mol with a barrier of only +1.8 kcal/mol. The formed hydrogen peroxide anion in the product structure is bent toward the bridgehead amine group and the transferred hydrogen points toward the nitrogen atom of the bridgehead amine N^B (see Figure 2). The assignment of the bound oxygen species as peroxide[16] is corroborated by the O−O bond length of 1.430 Å, which is typical for peroxides,[89,90] and the local spin of +0.80 a.u. on Fe_d, indicating that it is formally oxidized to +III. The dissociation of $OOH^{\bullet}$ from the product is energetically not favored ($\Delta E^{(4)}_{dissoc} = +24.6$ kcal/mol or $\Delta E^{(80)}_{dissoc} = +22.3$ kcal/mol). The dissociation of OOH^-, however, is energetically favored when the solvated reference state of the dissociated OOH^- is considered ($\Delta E^{(4)}_{dissoc} = +22.4$ kcal/mol or $\Delta E^{(80)}_{dissoc} = -5.7$ kcal/mol). The second

dx.doi.org/10.1021/ic501049z | Inorg. Chem. 2014, 53, 11890−11902

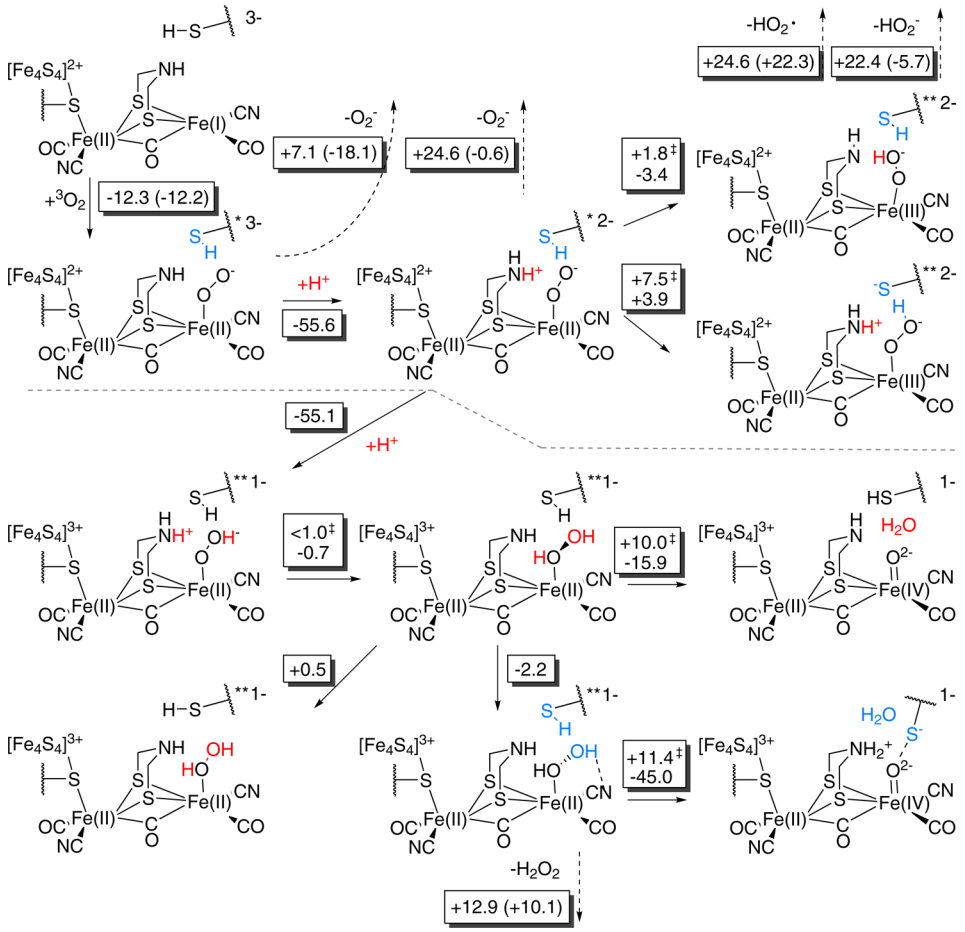

Figure 2. Oxygen activation reactions triggered by oxygen coordination to Fe_d and two successive proton transfer steps to the H cluster. The dashed line separates reactions induced by the first and second protonation reactions. Differences in electronic energies are given in kcal/mol. Reaction barriers are indicated by ‡. Ligand dissociation energies are given for both reference states ($\varepsilon = 80$ in parentheses). The charge on the upper right of every structure is the total charge of the system. One asterisk (*) on the upper right of a structure indicates a bound superoxide species, and two asterisks (**) indicate a bound peroxide species.

possible proton transfer is from the thiol to the distal oxygen atom with $[Fe_4S_4]^{2+}[Fe(II)Fe(III)]^{NH_2+/S^-}$–$OOH^-$ as product. This proton transfer is slightly endothermic (+3.9 kcal/mol) and has a barrier of +7.5 kcal/mol. The thiol is an acid too weak to protonate the bound O_2^- at this oxidation state. Bond length and local spin of coordinated HO_2^- are similar to the bond length and local spin in the first product ($[Fe_4S_4]^{2+}[Fe(II)Fe(III)]^{NH/SH}$–$OOH^-$).

The next proton transfer to the peroxide moiety is crucial, as water formation is, in principle, possible by proton transfer to the distal oxygen atom. The minimum-energy structures resulting after protonation, however, indicate that water formation competes with hydrogen peroxide formation. To find the favored product we must consider more than one conformation. The stable conformations that can be found starting with protonation of the bridgehead amine are shown in Figure 2. A hydrogen peroxide anion-bound species $[Fe_4S_4]^{3+}[Fe(II)Fe(II)]^{NH_2^+/SH}$–OOH with protonated bridgehead amine can be optimized. It is −55.1 kcal/mol more stable than $[Fe_4S_4]^{2+}[Fe(II)$-$Fe(II)]^{NH_2^+/SH}$–OO^-. The proton transfer to the H cluster triggers shift of a reduction equivalent from the cubane to the $[2Fe]_H$ subsite. This shift is reflected in the decrease of local spin in the cubane. Fe_p and Fe_d carry no local spin (0.00 a.u. and −0.02 a.u., respectively) and therefore they can be assigned the oxidation state +II. Proton transfer to the bound O_2H^- leads to a bound hydrogen peroxide, not to water, and is exothermic by −0.7 kcal/mol. Hydrogen peroxide formation is preferred to water formation because of the structure of the $[2Fe]_H$ subcluster. The transferred proton is spatially closer to O_p than to O_dH. We were not able to optimize a transition state for the proton transfer reaction but with a PES scan of the N^B–H distance, which resembles the reaction coordinate, we estimated the proton transfer barrier to be at most +1.0 kcal/mol.

In principle, water could be formed by disproportionation of the bound H_2O_2, that is, proton transfer from O_pH to O_dH. This reaction is exothermic by −15.9 kcal/mol but has a barrier of +10.0 kcal/mol, which is relatively high compared to other competing proton transfer reactions. Note that we were not able to find a direct proton transfer pathway from N^B to O_dH in $[Fe_4S_4]^{3+}[Fe(II)Fe(II)]^{NH_2^+/SH}$–$OOH^-$ to form water. Water formation appears to proceed only via the peroxide formation pathway. Once water is formed, it remains attached to the cluster because of hydrogen bonding. In the enzyme the water molecule might form hydrogen bonds to other hydrogen bond acceptors and could be removed from the active site more facile.

For $[Fe_4S_4]^{3+}[Fe(II)Fe(II)]^{NH/SH}$–$O_2H_2$ a second, −2.2 kcal/mol more stable conformation exists, in which the proton at the distal oxygen atom forms a hydrogen bond to the cyanide ligand at Fe_d (Figure 2). Water formation is possible by proton transfer from the thiol to the distal oxygen atom in this

dx.doi.org/10.1021/ic501049z | Inorg. Chem. 2014, 53, 11890−11902

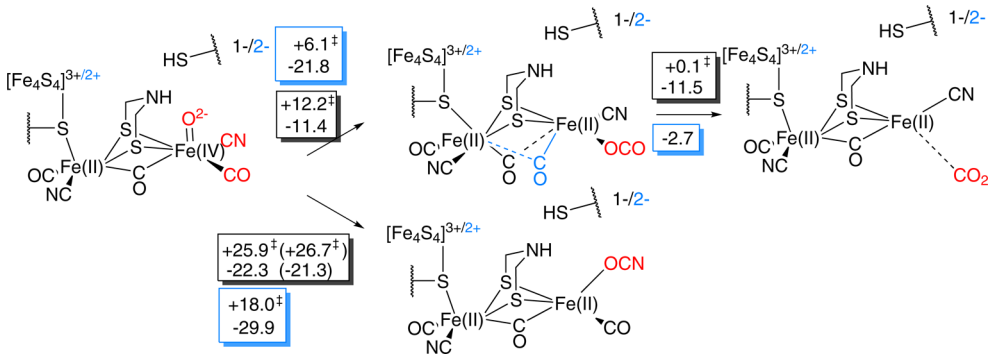

Figure 3. Oxygen insertion reactions of a putative iron-oxo species. Differences in electronic energies are given in kcal/mol. Reaction barriers are indicated by ‡. The charge on the upper right of every structure is the total charge of the system. Black charges and boxes correspond to the unreduced model system; blue charges and boxes correspond to model systems reduced by one electron. The reaction energies in parentheses correspond to an alternative conformation of the thiol S−H.

conformation (see Figure 2). In this process, which has a barrier of +11.4 kcal/mol and is exothermic by −45.0 kcal/mol, the O−O bond is cleaved and the proton at the proximal O atom is transferred back to N^B and the resulting Fe(IV)=O^{2-} species is in close contact to the thiolate S^-.

Hence, if a proton is available, hydrogen peroxide formation is very likely. H_2O_2 dissociation therefore directly competes with the release of water which, in turn, results in a highly oxidized and reactive Fe(IV)=O^{2-} species.

H_2O_2 dissociation from $[Fe_4S_4]^{3+}[Fe(II)Fe(II)]^{NH/SH}$−$O_2H_2$ is energetically unfavored ($\Delta E^{(4)}_{dissoc}$ = +12.9 kcal/mol or $\Delta E^{(80)}_{dissoc}$ = +10.1 kcal/mol).

If water formation occurs upon protonation of the coordinated O_2, the $[2Fe]_H$ subcluster is transformed into an iron-oxo species, $[Fe_4S_4]^{3+}[Fe(II)Fe(IV)]^{NH/SH}$=$O^{2-}$, with decreased local spin in the cubane as compared to the hydrogen-peroxide-bound intermediate. The local spin on Fe_p is +1.11 a.u. and on the remaining oxygen atom +0.85 a.u. These spin populations point to a formal description of the Fe−O moiety as Fe(III)−O^- or Fe(IV)=O^{2-}. The Fe−O bond length of 1.693 Å is slightly larger than for comparable Fe(IV)=O^{2-} species like Compound I in cytochrome P450 (according to density functional theory (DFT) calculations: 1.65[91] or 1.63[92] Å) or a nonheme Fe(IV)=O^{2-} complex (measured: 1.65 Å[93]). Note, however, that in the $[Fe_4S_4]^{3+}[Fe(II)Fe(IV)]^{NH/SH}$=$O^{2-}$, the oxo ligand is coordinated by water upon which a bond elongation can be expected. We therefore favor the Fe(IV)=O^{2-} description instead of Fe(III)−O^-, as discussed in our previous study.[16]

3.2. Reactivity of the Terminal Iron-Oxo Species. The iron-oxo species $[Fe_4S_4]^{3+}[Fe(II)Fe(IV)]^{NH/SH}$=$O^{2-}$, mentioned in the last section, features different competing reaction channels. Oxygen reduction requires additional protons. If proton transfer to the active site is not fast enough, oxygen insertion into the Fe_d−CN^- or Fe_d−CO bonds might occur, which offers a pathway for H cluster degradation via disintegration of the $[2Fe]_H$ subsite as discussed in refs 13 and 16. These insertion reactions are shown in Figure 3. Insertion into the Fe−CN^- bond to form a cyanate ligand (OCN^-) is highly exothermic (−22.3 kcal/mol). This reaction has, however, a considerable barrier of +25.9 kcal/mol. In the transition state, the Fe−CN^- bond is slightly elongated to 1.939 Å compared to 1.927 Å in the reactant structure. The oxygen atom is bent toward the CN^- ligand. In the product structure, the cyanate ligand is approximately in the apical position *trans* to the bridging CO. The cubane remains oxidized, but there is no local spin remaining on the cyanate ligand and the local spin on Fe_d is only −0.02 a.u. Hence, cyanate formation is accompanied by reduction of Fe_d. Note that the reactant might exist in a different conformation where the thiol S−H points toward the coordinated oxo atom (compare Figure 3). It is 1.9 kcal/mol more stable but the barrier for OCN^- formation is about the same. The orientation of the thiol S−H has thus no influence on the interpretation and will not be considered for further oxo-insertion reactions.

In comparison to OCN^- formation, CO_2 formation by O-insertion into the Fe_d−CO bond is, with −11.4 kcal/mol, less exothermic. However, the barrier of +12.2 kcal/mol is considerably smaller than for the insertion into the Fe−CN^- bond. As a consequence, CO_2 formation should be faster than OCN^- formation. In the optimized product structure the CO_2 is still coordinated to Fe_d and the formerly bridging CO resides at Fe_p. A PES scan of the Fe_d−CO distance indicates that complete CO_2 dissociation is exothermic and has a negligibly low barrier (estimated to be approximately +0.1 kcal/mol). The facile CO_2 formation and dissociation from the cluster offers a putative H cluster degradation pathway as discussed in refs 13 and 16. Cluster degradation could be prevented by protonation of the oxo ligand. Additional proton supply would therefore be crucial for maintaining the integrity of the $[2Fe]_H$ subsite.

3.3. Further Proton Supply to the H Cluster. To fully reduce O_2 to water, two additional external protons are required. Again, we assume initial protonation of the bridgehead amine to $R_2N^BH^+_2$. The resulting structure does not correspond to a minimum on the PES and the proton is directly transferred to the coordinated oxygen atom resulting in a hydroxo ligand, $[Fe_4S_4]^{3+}[Fe(II)Fe(IV)]^{NH/SH}$−$OH^-$ (see Figure 4). Protonation, with the hydroxy ligand-bound species as product, is exothermic by −26.8 kcal/mol, which is significantly less exothermic than the first two protonation reactions (−55.6 and −55.1 kcal/mol, respectively). In $[Fe_4S_4]^{3+}[Fe(II)Fe(IV)]^{NH/SH}$−$OH^-$, the local spin on Fe_d is +0.83 a.u., which is less than in the iron-oxo species (+1.11 a.u.). We still assign the formal oxidation states to be Fe_p(II)Fe_d(IV), and the charge state of the cubane to be +3 elementary charges. The proton of the thiol is oriented away from the hydroxo ligand. An alternative conformation with the thiol proton pointing above the hydroxo ligand is higher in energy by +6.0 kcal/mol. Dissociation of a hydroxyl radical from this species appears to be unlikely to occur ($\Delta E^{(4)}_{dissoc}$ = +42.8 kcal/mol and $\Delta E^{(80)}_{dissoc}$ = +41.1 kcal/mol). Dissociation of a hydroxide anion is energetically even more unfavored ($\Delta E^{(4)}_{dissoc}$ = +86.2 kcal/mol and $\Delta E^{(80)}_{dissoc}$ = +55.6 kcal/mol). Note that in the product structure

dx.doi.org/10.1021/ic501049z | *Inorg. Chem.* 2014, 53, 11890−11902

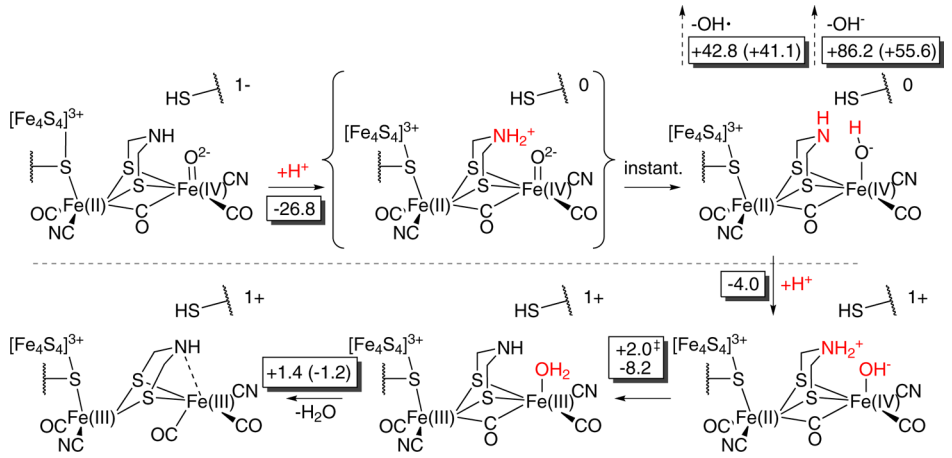

Figure 4. Reactions induced by the third and fourth proton transfer to the active site. Differences in electronic energies are given in kcal/mol. Reaction barriers are indicated by ‡. The dashed line separates the different protonation states. The charge on the upper right of every structure is the total charge of the system.

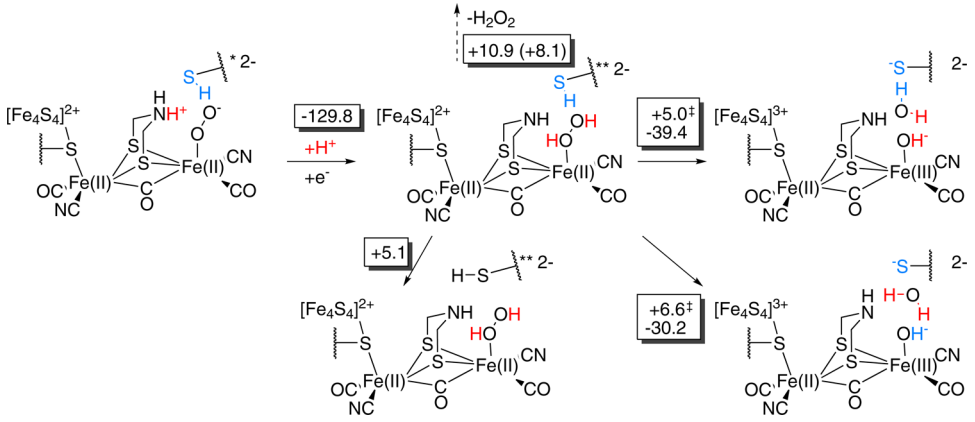

Figure 5. Reactions at the $[2Fe]_H$ subsite following the second proton transfer coupled to reduction of the model system. Differences in electronic energies are given in kcal/mol. Reaction barriers are indicated by ‡. The H_2O_2 dissociation energy is given for both reference states (ε = 80 in parentheses). The charge on the upper right of every structure is the total charge of the system. One asterisk (*) on the upper right of a structure indicates a bound superoxide species, and two asterisks (**) indicate a bound peroxide species.

of both dissociation reactions the sulfur atom of Cys299 coordinates Fe_d, which requires a distortion of the $[2Fe]_H$ subcluster with respect to the cubane. This might be prohibited in the enzyme by the salt bridge between Lys358 and the cyanide ligand of Fe_d.[77]

Water formation would require a second proton transfer to the hydroxo ligand. Protonation of the bridgehead amine is exothermic by only −4.0 kcal/mol. In our model system the cluster is negatively charged in the active oxidation states. This negative charge is compensated or screened in the protein. Hence, protonation energies of our isolated cluster are artificially exothermic due to charge compensation. Therefore, the low exothermicity of this protonation step is an indication that it might not happen in the enzyme. Furthermore, it was not possible to converge states with antiferromagnetically coupled Fe atoms in the cubane (two Fe atoms spin up and two Fe atoms spin down) after proton addition. This might indicate that this redox state is not accessible. As a consequence of the different coupling pattern in the cubane, the given oxidation states are not derived from the Kohn−Sham wave function, but simply fulfill a labeling purpose. Proton addition to the bridgehead amine group results in $[Fe_4S_4]^{3+}[Fe(II)Fe(IV)]^{NH_2^+/SH}-OH^-$. Proton transfer to form water ($[Fe_4S_4]^{3+}[Fe(III)Fe(III)]^{NH/SH}-OH_2$) is exothermic by −8.2 kcal/mol and has a low (classical) barrier of +2.0 kcal/mol. Water dissociation from $[Fe_4S_4]^{3+}[Fe(III)Fe(III)]^{NH/SH}-OH_2$ is endothermic by +1.4 kcal/mol or exothermic by −1.2 kcal/mol for the cavity or solvated reference state, respectively.

4. O_2 ACTIVATION WITH SIMULTANEOUS REDUCTION REACTIONS FOLLOWING THE SECOND PROTON TRANSFER

We now consider how the picture for O_2 reactions at the $[2Fe]_H$ subsite discussed in the previous section changes when electron transfer to the H cluster is possible at the same time. After coordination of O_2, the $[2Fe]_H$ subcluster is in the formal oxidation state $Fe_p(II)Fe_d(II)$ (corresponding to a coordinated superoxide). To keep the H cluster formally in this oxidation state electrons have to be supplied before or simultaneously with the second protonation step. As a consequence, the reactions starting after the second protonation step proceed for a more reduced model system compared to the situation described in Section 3 (see Figure 5). Note that reduction by one electron results in the same electron count as starting from H_{red}.

Proton-coupled electron transfer to $[Fe_4S_4]^{2+}[Fe(II)Fe(II)]^{NH_2^+/SH}-OO^-$ is exothermic by −129.8 kcal/mol. In the resulting structure the bridgehead's proton is transferred to the proximal oxygen atom to form the hydrogen peroxide bound product $[Fe_4S_4]^{2+}[Fe(II)Fe(II)]^{NH/SH}-O_2H_2$ (O−O bond length: 1.484 Å). In $[Fe_4S_4]^{2+}[Fe(II)Fe(II)]^{NH/SH}-O_2H_2$ the conformation with thiol S−H pointing to the distal oxygen atom is

dx.doi.org/10.1021/ic501049z | Inorg. Chem. 2014, 53, 11890−11902

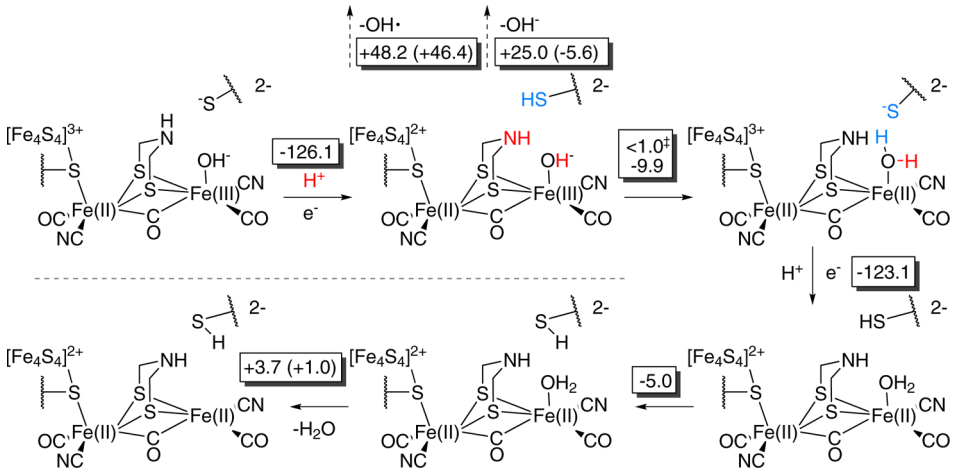

Figure 6. Reactions initialized by the third and fourth proton transfer steps to the active site coupled with electron transfers. Differences in electronic energies are given in kcal/mol. Reaction barriers are indicated by ‡. The dashed line separates the different protonation states. The charge on the upper right of every structure is the total charge of the system.

−5.1 kcal/mol more stable than the conformation where the thiol S−H is oriented away from the coordinated H_2O_2 (cf. Figure 5). In contrast to the scenario without reduction, the cubane remains in charge state +2 and Fe_p and Fe_d are in oxidation state +II. These assignments are supported by the small local spin of +0.18 a.u. on Fe_d and of +0.10 a.u. on Fe_p. There is no local spin on the coordinated hydrogen peroxide and H_2O_2 dissociation is energetically unfavored ($\Delta E^{(4)}_{dissoc}$ = +10.9 kcal/mol or $\Delta E^{(80)}_{dissoc}$ = +8.1 kcal/mol).

Again, water can be formed in competition to hydrogen peroxide release. O−O bond cleavage by proton transfer from O_p to O_dH (H_2O_2 disproportionation) has a barrier of +6.6 kcal/mol at this oxidation state and leads to the formation of water and, simultaneously, the thiol proton is transferred to O_p to form a hydroxo ligand. This reaction is exothermic by −30.2 kcal/mol. Hence, in this reaction step an iron-oxo species is avoided. Water formation by proton transfer from the thiol to O_dH has an even lower barrier of only +5.0 kcal/mol and is exothermic by −39.4 kcal/mol. The reaction avoids formation of an iron-oxo species as well. The product is similar to the product of the H_2O_2 disproportionation but has a different configuration of the bridgehead amine, resulting from the different reaction pathway (see Figure 5). It features a bound hydroxo ligand and the water molecule remains attached to the cluster because of hydrogen bonding.

Although both water formation reactions avoid the iron-oxo intermediate, a stable iron-oxo structure, $[Fe_4S_4]^{2+}$[Fe(II)-Fe(IV)]$^{NH/SH}$=O^{2-}, can be obtained after removal of water from the system. Here, we label the cubane to be in charge state +2 (this is not unambiguously supported by the local spins), in contrast to the iron-oxo species without reduction steps, where it is in charge state +3. In the iron-oxo species, local spin on Fe_d is +0.98 a.u. and the bound oxygen atom has a local spin of +0.75 a.u., indicating an oxidized iron atom and reduced oxygen atom, similar to the scenario without reduction steps. The oxidation state assignment is corroborated by a Fe−O bond length of 1.717 Å. The local spins in the proximal cubane layer are reduced, indicating an electron shift from the cubane to the $[2Fe]_H$ subsite.

We now consider the same insertion reactions of the iron-oxo species as in Section 3.2, but with a model system reduced by one electron. At this oxidation state, CO_2 formation by insertion into the Fe−CO bond has a barrier of only +6.1 kcal/mol (compared to +12.2 kcal/mol without reduction) and is exothermic by −21.8 kcal/mol (see Figure 3). CO_2 dissociation from the product structure is exothermic (−2.7 kcal/mol). Hence, formation of the iron-oxo species in the one-electron reduced state enables a faster cluster degradation pathway via CO_2 formation compared to the more oxidized system.

OCN^- formation by oxygen insertion into the Fe−CN^- bond is exothermic by −29.9 kcal/mol (−22.3 kcal/mol without reduction) but still has a large barrier of +18.0 kcal/mol (+25.9 kcal/mol without reduction). The structure of the product is similar to the structure obtained without simultaneous electron transfer steps and is depicted in Figure 3. The local spins in the cubane are increased again, compared to the reactant. The local spin on Fe_d is +0.87 a.u., whereas the local spin on the cyanate is nearly zero. The coordination sphere of Fe_d is distorted compared to the reactant. The OCN^- ligand resides in between the apical and basal coordination sites, which were occupied by the oxo and cyanide ligands in the reactant.

Additional proton-coupled electron transfers to the active site after release of the first water molecule leads to full reduction of oxygen (see Figure 6). The first reduction and protonation results in the formation of $[Fe_4S_4]^{2+}$[Fe(II)Fe(III)]$^{NH/SH}$−OH^-, and is exothermic by −126.1 kcal/mol. The thiol S−H is oriented away from the bound hydroxo ligand in the product structure. There is still local spin on Fe_d (+0.94 a.u.) and small local spin excess on the oxygen atom of the hydroxo ligand (+0.25 a.u.). The cubane can be assigned a charge state of +2. Dissociation of a hydroxyl radical is unlikely ($\Delta E^{(4)}_{dissoc}$ = +48.2 kcal/mol and $\Delta E^{(80)}_{dissoc}$ = +46.4 kcal/mol). Also, dissociation of a hydroxide anion is energetically unfavored for the cavity reference state ($\Delta E^{(4)}_{dissoc}$ = +25.0 kcal/mol), but energetically slightly favored for the solvated reference state ($\Delta E^{(80)}_{dissoc}$ = −5.6 kcal/mol). When the thiol S−H is oriented toward the hydroxo ligand the thiol proton can be transferred to the hydroxo ligand to form H_2O ($[Fe_4S_4]^{3+}$[Fe(II)Fe(II)]$^{NH/S^-}$−OH_2). In the product structure, the cubane presumably is in charge state +3 (local spins are decreased) and there is only little local spin on the thiolate sulfur atom (−0.27 a.u.). Fe_p and Fe_d carry no local spin. The water formation reaction is exothermic by −9.9 kcal/mol and an upper bound for the barrier was estimated by a PES scan to be smaller than +1.0 kcal/mol.

dx.doi.org/10.1021/ic501049z | Inorg. Chem. 2014, 53, 11890−11902

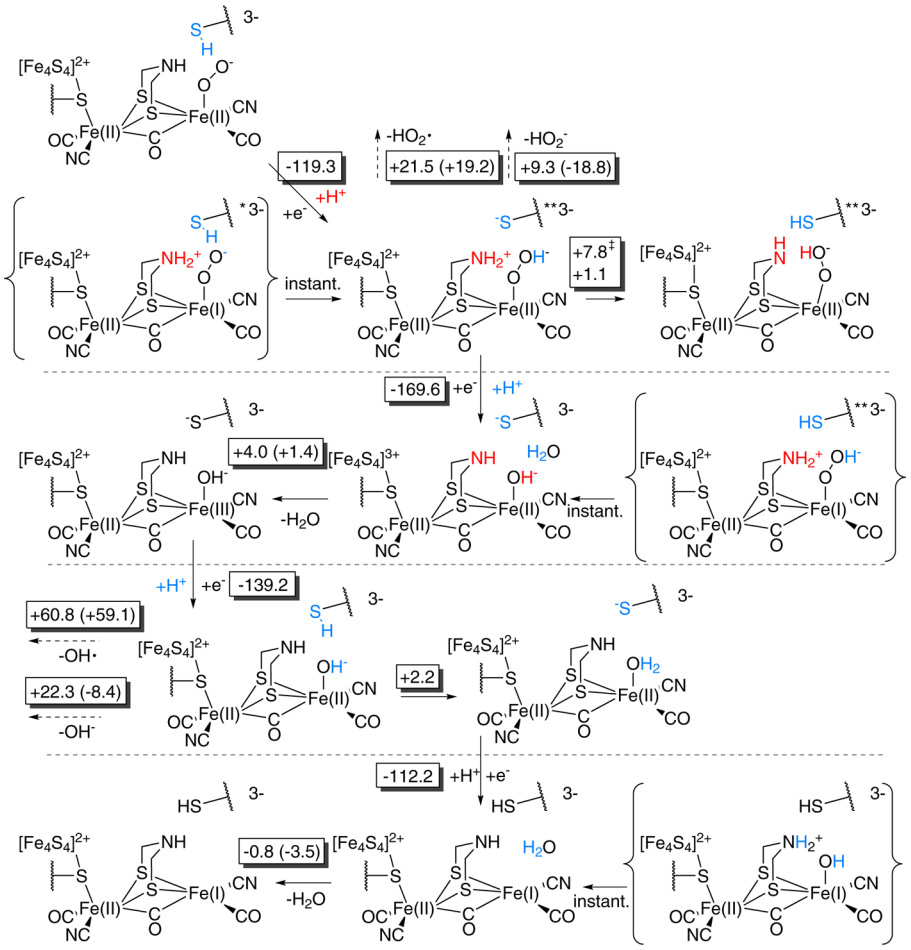

Figure 7. O_2 reactions at the H cluster if proton-coupled electron transfer to the active site is considered. Differences in electronic energies are given in kcal/mol. Reaction barriers are indicated by ‡. Ligand dissociation energies are given for both reference states (ε = 80 in parentheses). The dashed lines separate the different protonation states. The charge on the upper right of every structure is the total charge of the system. One asterisk (*) on the upper right indicates a bound superoxide species and two asterisks (**) a bound peroxide species.

Proton-coupled electron transfer to $[Fe_4S_4]^{3+}$[Fe(II)-Fe(II)]$^{NH/S^-}$−OH_2 is exothermic by −123.1 kcal/mol (Figure 6). The resulting product $[Fe_4S_4]^{2+}$[Fe(II)Fe(II)]$^{NH/SH}$−OH_2 has reduced local spins in the cubane. Fe_p and Fe_d have local spins of +0.20 a.u. and 0.31 a.u., respectively. A −5.0 kcal/mol more stable conformation with the SH pointing toward the coordinated water molecule can be found. Water dissociation from the final species is energetically slightly unfavored by +3.7 kcal/mol or +1.0 kcal/mol for ε = 4 or ε = 80, respectively.

5. O_2 ACTIVATION AT THE $[2FE]_H$ SUBSITE BY FOUR PROTON-COUPLED ELECTRON TRANSFER STEPS

Now we investigate a scenario, in which proton transfer to the H cluster is always coupled to simultaneous electron transfer. Since we assume oxygen coordination to H_{ox} (Fe_p(II)Fe_d(I)), complete O_2-degradation with proton-coupled electron transfer leads to a water-bound H cluster in H_{ox} oxidation state as final product and can be considered as the other extreme scenario in contrast to proton supply without reduction (Section 3).

The reactions triggered by only proton-coupled electron transfer steps after O_2 coordination to Fe_d are shown in Figure 7. With reduction coupled already to the first proton transfer, the initial structure (proton at N^B) is not a stable minimum structure and structure optimization directly converges to a product where the thiol proton (not the proton of the ammonium group) is transferred to the distal oxygen atom of the coordinated O_2 ($[Fe_4S_4]^{2+}$[Fe(II)Fe(II)]$^{NH_2+/S^-}$−OOH^-, compare Figure 7). This reaction is exothermic by −119.3 kcal/mol. In $[Fe_4S_4]^{2+}$[Fe-(II)Fe(II)]$^{NH_2+/S^-}$−OOH^-, one proton of the ammonium group points toward the proximal oxygen atom of the coordinated OOH^- and has a slightly elongated N^B−H bond (1.124 Å vs 1.104 Å for the other N−H bond). The O−O bond length is 1.492 Å, corresponding to a hydrogen peroxide anion. Dissociation of $OOH^•$ is unlikely ($\Delta E^{(4)}_{dissoc}$ = +21.5 kcal/mol or $\Delta E^{(80)}_{dissoc}$ = +19.2 kcal/mol). Dissociation of OOH^-, however, is energetically only unfavored for the ε = 4 reference state ($\Delta E^{(4)}_{dissoc}$ = +9.3 kcal/mol) and strongly favored for the hydrated reference state ($\Delta E^{(80)}_{dissoc}$ = −18.8 kcal/mol).

For the OOH^--bound intermediate another minimum structure ($[Fe_4S_4]^{2+}$[Fe(II)Fe(II)]$^{NH/SH}$−OOH^-, O−O bond length: 1.447 Å) can be found where the proton of the ammonium group is transferred to the distal oxygen atom of the bound oxygen, similar to the reaction without reduction (compare $[Fe_4S_4]^{2+}$-[Fe(II)Fe(III)]$^{NH/SH}$−OOH^-, Figure 2, upper right). The oxygen molecule is bent toward the bridgehead amine group. This structure is by +1.1 kcal/mol less stable and the barrier for its formation is +7.8 kcal/mol. In both structures, the cubane is in charge state +2 and there is nearly no spin polarization on Fe_p and Fe_d. Especially the fact that the thiol proton is transferred more easily to the bound oxygen than the ammonium proton

dx.doi.org/10.1021/ic501049z | Inorg. Chem. 2014, 53, 11890−11902

raises the question whether water or hydrogen peroxide formation would be possible already at this stage. However, starting structures with a proton transferred from NH_2^+ to O_p starting from $[Fe_4S_4]^{2+}[Fe(II)Fe(II)]^{NH_2+/S^-}-OOH^-$ or with a proton transferred from SH to O_dH starting from $[Fe_4S_4]^{2+}[Fe(II)Fe(II)]^{NH/SH}-OOH^-$ converged back to the corresponding reactant structures indicating that water or H_2O_2 formation do not occur at this stage.

If the second electron transfer is coupled to proton transfer, water is formed directly. Starting structures with protonated bridgehead amine group directly converge to intermediates where the thiol proton is transferred to the distal oxygen atom to form water from the bound hydrogen peroxide anion. Simultaneously, one proton of the bridgehead ammonium group is transferred to the proximal oxygen atom forming a hydroxo ligand. With $[Fe_4S_4]^{2+}[Fe(II)Fe(II)]^{NH_2+/S^-}-OOH^-$ as reactant, this reaction is exothermic by −169.6 kcal/mol (cf. Figure 7). The direct formation of the hydroxo ligand avoids creation of an iron-oxo intermediate. The water molecule stays attached to the $[2Fe]_H$ subsite via hydrogen bonding. In the product structure, the local spins in the cubane are decreased, indicating a shift of electron density from the cubane to the $[2Fe]_H$ subcluster. The local spin on Fe_p and Fe_d is zero. Water dissociation is energetically slightly unfavored ($\Delta E^{(4)}_{dissoc}$ = +4.0 kcal/mol $\Delta E^{(80)}_{dissoc}$ = +1.4 kcal/mol). In the resulting hydroxo ligand-bound species the local spins in the cubane are increased again (charge state +2) and the local spins on Fe_p and Fe_d are −0.04 a.u. and +0.70 a.u., respectively.

Starting structures, corresponding to an iron-oxo species were no minimum structures on the PES, and the thiol proton is transferred to the bound oxygen atom to form a hydroxo ligand. Hence, at this oxidation state of the H cluster the iron-oxo species can apparently be avoided by direct protonation. CO_2 or OCN^- formation are therefore unlikely to occur.

The third proton-coupled electron transfer step to the H cluster is exothermic by −139.2 kcal/mol and leads to $[Fe_4S_4]^{2+}[Fe(II)Fe(II)]^{NH/SH}-OH^-$. Here, the cubane is in charge state +2 and the local spins on Fe_p and Fe_d are nearly zero (−0.01 a.u. on Fe_d and 0.00 a.u. on Fe_p). Again, dissociation of $OH^\bullet$ is unlikely with $\Delta E^{(4)}_{dissoc}$ = +60.8 kcal/mol or $\Delta E^{(80)}_{dissoc}$ = +59.1 kcal/mol, while dissociation of OH^- is energetically favorable only for the solvated reference state ($\Delta E^{(4)}_{dissoc}$ = +22.3 kcal/mol vs $\Delta E^{(80)}_{dissoc}$ = −8.4 kcal/mol).

Formation of a water ligand by proton transfer from the thiol to the hydroxo ligand is endothermic by only +2.2 kcal/mol resulting in $[Fe_4S_4]^{2+}[Fe(II)Fe(II)]^{NH/S^-}-OH_2$. The next proton and electron addition, which is exothermic by −112.2 kcal/mol, would lead to cleavage of the Fe_d-H_2O bond. The water molecule remains attached to the complex via hydrogen boding and water dissociation is energetically slightly favored ($\Delta E^{(4)}_{dissoc}$ = −0.8 kcal/mol or $\Delta E^{(80)}_{dissoc}$ = −3.5 kcal/mol). After water dissociation the H_{ox} state ($[Fe_4S_4]^{2+}[Fe(II)Fe(I)]^{NH/SH}$) is recovered—ready for catalytic action. Hence, with sufficiently many reduction equivalents and protons available, oxygen could be oxidized to water. Of course, harmful side reactions, like ROS formation, are still possible but we would expect their ratio, compared to H_2O formation, to be smaller.

6. DISCUSSION

6.1. Comparison to Previous Results. Several computational studies on [FeFe] hydrogenases from our group and others have been published. However, there are slight modulations in reaction energies given in the different studies, which deserves a comment.

H cluster models can have subtle differences. Important factors are (i) the oxidation state of both iron atoms. (ii) The size of the model and the crystal structure where it was derived from. (iii) Within the cluster approach the model system is usually fixed in space at bonds linking to the protein. This fixation (atoms or bond lengths and orientations) has to be kept consistent for the calculation of reaction energies but can vary between studies. (iv) The identity of the central atom of the bridging ligand and its protonation state. The fourth topic was discussed controversially and several models were applied: 1,3-propanedithiolate,[76,94] dithiomethyl ether,[16] di(thiomethyl)amine.[24,77,94,95] (v) There are different antiferromagnetic coupling patterns possible for the cubane and of the cubane to the $[2Fe]_H$ subsite. The choice of the coupling pattern can affect the results. A large effect (>6 kcal/mol) of the coupling pattern on energies was only found for species where oxygen attacked the cubane.[79] The iron atoms of the cubane can also be treated as low spin Fe.[16] (vi) Structures were optimized with and without the COSMO model for solvation. (vii) Reaction energies can be calculated differently. For example, H_2O_2 formation energy can be calculated as HO_2^- dissociation and successive HO_2^- protonation.[79] Then, the energy of this reaction depends on the reference state chosen for the proton (energy of the solvated proton) and thus differs from the way H_2O_2 dissociation is investigated in this work. The choice of the reference state of the proton can then yield very exothermic "net" dissociation energies of −60 kcal/mol and more as reported in ref 79 (see Table 1).

Apart from these factors the reaction energies are dependent on the electronic structure method. In this study we applied the BP86 exchange-correlation functional.[65,66] It has the advantage of being computationally efficient and reliably yielding good structures for Fe−S systems[16,96,97] also in comparison to the B3LYP[98−100] exchange-correlation functional. Still, the accuracy of DFT methods is limited (errors can be up to 10 kcal/mol and even larger[101]) and reaction energies can vary between different functionals. However, we observed overall consistent results with B3LYP and BP86 (B3LYP always yields higher barriers[77]) in previous studies and energy variations did not affect the chemical conclusions.[16,24,77,79]

Furthermore, the calculation of dissociation energies depends on the inclusion of entropic effects and on the chosen reference state of the dissociated ligand (protein cavity or fully solvated), as discussed in Section 2. For a comparison we added the entropy correction and reference state dependence to the ROS dissociation energies (dissociated ligand calculated with ε = 4 and ε = 80) published in ref 79. The original ROS dissociation energies of ref 79 and the corrected values are shown in Table 1. The dissociation of superoxide from H_{ox} is the only reaction that was also calculated in this work and is therefore given in Table 1 for comparison as well. Note that for this reaction, we obtain a different reaction energy calculated from the electronic energies (i.e., +18.1 kcal/mol compared to +12.9 kcal/mol in ref 79), which originates from a different orientation of the thiol group compared to the structure reported in ref 79.

6.2. ROS Dissociation Reactions. We explored a cascade of activation reactions of O_2 coordinated to Fe_d. Several intermediates in this cascade correspond to a bound reactive oxygen species which could detach from the $[2Fe]_H$ subsite and react with the nearby cubane, as observed in theory and experiment.[15,24] We observed that most ROS dissociation reactions are energetically unfavored for the oxidized systems investigated.

Table 1. Reaction Energies of ROS Dissociation Reactions of Ref 79 Augemented by Entropy Corrections (in kcal/mol)

reactants	dissociating ROS	$\Delta E_{el}^{(4)}$ [a]	$\Delta E_{dissoc}^{(4)}$ [b]	$\Delta E_{dissoc}^{(80)}$ [b]
$[Fe_4S_4]^{2+}[Fe(II)Fe(I)] - O_2^-$	O_2^-	−19.6[79]	−30.7	−55.9
$[Fe_4S_4]^{2+}[Fe(II)Fe(II)] - O_2^-$	O_2^-	+12.9[79]	+1.8	−23.4
$[Fe_4S_4]^{2+}[Fe(I)Fe(II)] - O_2H^-$	O_2H^-	−11.2[79]	−23.9	−52.0
$[Fe_4S_4]^{2+}[Fe(II)Fe(II)] - O_2H^-$	O_2H^-	+18.6[79]	+5.9	−22.2
$[Fe_4S_4]^{2+}[Fe(II)Fe(II)] - O_2H^-$	$O_2H^\bullet$	+31.5[79]	+19.0	+16.5
$[Fe_4S_4]^{2+}[Fe(II)Fe(III) - O_2H^-$	$O_2H^\bullet$	+30.0[79]	+17.5	+15.2
$[Fe_4S_4]^{2+}[Fe(II)Fe(I)] - O_2H^- + H^+$	O_2H_2	−86.9[79]	−100.1	−102.9
$[Fe_4S_4]^{2+}[Fe(II)Fe(II)] - O_2H^- + H^+$	O_2H_2	−60.9[79]	−74.1	−76.9
this work				
$*[Fe_4S_4]^{2+}[Fe(II)Fe(II)]^{NH/SH} - O_2^-$	O_2^-	+18.1	+7.1	−18.2

[a]Original data of Ref 79. [b]Translational and rotational entropy corrections added (indicated with subscript "dissoc") for cavity ($\varepsilon = 4$) and solvated reference state ($\varepsilon = 80$). *The reactant structure has a different orientation of the thiol group compared to ref 79, which is the reason for the different reaction energy.

Only for anionic ROS an energetically favored dissociation is obtained for the fully solvated reference state (dissociated ROS calculated with $\varepsilon = 80$). Thus, dissociation of O_2^- and HO_2^- is likely. H_2O_2 dissociation is energetically unfavored by +8 to +12 kcal/mol, depending on the oxidation state of the H cluster. We expect H_2O_2 dissociation to be still possible. In our previous work we found that for more reduced systems O_2^-, HO_2^- and H_2O_2 dissociation are energetically favored[79] (compare Table 1).

6.3. Oxygen Activation. Oxygen activation chemistry, similar to the reactions discussed here, is well understood for other iron-containing enzymes, which are known for producing ROS in biology.[102] Heme proteins, like the well characterized cytochrome P450, oxidize organic compounds by activating oxygen via successive reduction and protonation reactions, and hydrogen peroxide or superoxide are side products in this process.[103] There are also enzymes with nonheme Fe(II) centers known, which catalyze a variety of oxidation reactions (i.e., oxygenases) involving reactive oxygen species bound to Fe.[104−106] Highly oxidized iron-oxo species are common intermediates in these catalytic cycles.[107] A similar oxygen activation mechanism, where a nearby acid protonates an activated coordinated oxygen molecule and finally reduces it to water, was recently demonstrated for electron-deficient cobalt(II) hangman porphyrins.[108] Thus, a group capable of proton transfer in the vicinity of the active site can promote oxygen activation.[108]

[FeFe] hydrogenases fulfill several prerequisites for oxygen activation. (i) They possess a Fe(II) center with a vacant coordination site. (ii) Reduction reactions by two electrons are possible, and (iii) protons can be transported to the active site.[104] The detailed kinetics of the reaction steps which ultimately lead to ROS formation and potential H cluster damage were not known.

The dissociation reactions for ROS compete with further reduction steps to finally form two water molecules, a formally complete reduction and detoxification of O_2. On the pathway to water formation, we identify two major branching points where water formation directly competes with harmful side reactions, which could explain the cluster degradation observed in experiment.[15] The first branching point is the second proton transfer via the bridgehead amine to yield Fe-bound hydrogen peroxide. In the first and second scenario investigated, this step leads to hydrogen peroxide and not to water formation. Proton transfer from O_pH to O_dH, to form an iron-oxo species and water, will be exothermic and will have barriers on the order of +10 kcal/mol without reduction steps and of +6 kcal/mol if the system is reduced by one electron. It is therefore decisive for the reaction events to follow whether either H_2O_2 dissociates (ROS formation) or the H_2O_2 bound species is persistent enough to be converted to water and an iron-oxo species. H_2O_2 dissociation would open the way for Fenton-type reactions (H_2O_2 cleaved to water and production of highly reactive hydroxyl radicals, catalyzed by Fe(II)[109]). H_2O_2 dissociation is energetically only slightly unfavored (by about +10 kcal/mol). Hence both processes (water plus iron-oxo formation or H_2O_2 dissociation) may happen.

The iron-oxo species that is formed after water dissociation is the second potential branching point. In the one-electron reduced system ($[Fe_4S_4]^{2+}[Fe(II)Fe(II)]^{NH/SH}-O_2H_2$) hydrogen peroxide cleavage directly leads to hydroxo ligand formation and the iron-oxo intermediate might not occur. Still, a stable iron-oxo species can be optimized after water removal from the system. Starting from this iron-oxo species, OCN^- formation by oxygen insertion into the Fe−CN^- bond is unlikely because of the high reaction barrier that is about +18 to +26 kcal/mol, dependent on the oxidation state. CO_2 formation by oxygen insertion into the Fe−CO bond is, however, feasible with a barrier of +12.2 kcal/mol without reduction and of only +6.1 kcal/mol for a by one electron reduced H cluster. If an additional proton is supplied to the iron-oxo species, hydroxo ligand formation is spontaneous. Hence, proton transfer will be essential to prevent damaging CO_2 formation by an iron-oxo species. However, without additional reduction equivalents the third and fourth proton transfers to the active site appear to be energetically not favored.

We find hydroxyl radical dissociation to be energetically unfavored for all investigated oxidation states. However, if $OH^\bullet$ is formed, sulfur oxygenation and other degradation reactions presumably will be strongly exothermic, leading to an overall exothermic "net" reaction (dissociation and sulfoxygenation). Dissociation of a hydroxide anion is energetically strongly favored for the scenario without reductions and slightly favored for the second scenario, if the solvated reference state is considered.

If the first and second proton transfer are coupled to electron transfer, water will be formed directly, and simultaneously,

the oxo ligand will be protonated by the thiol group of Cys299, which yields a hydroxo ligand coordinated to Fe_d. This prevents CO_2 or OCN^- formation. As a consequence, constant proton and electron supply to the H cluster facilitates water release to successfully compete with ROS formation. The reduction of O_2 to water would follow a mechanism similar to that of certain [NiFe] hydrogenases, which achieve oxygen tolerance by complete O_2 reduction (type II, see Introduction).

In this context, it is interesting to note that Goldet et al. electrochemically measured and compared inhibition kinetics of the [FeFe] hydrogenases from *Desulfovibrio desulfuricans* (DdHydAB), *Clostridium acetobutylicum* (CaHydA) and *Chlamydomonas reinhardtii* (CrHydA1).[20] One of their observations was that under H_2-oxidizing conditions, that is, at a potential of −0.05 V versus standard hydrogen electrode (SHE), the O_2 inhibition rate anticorrelates with catalytic H_2 oxidation activity. The oxygen inhibition rate decreases in the following order: DdHydAB > CrHydA1 > CaHydA. Furthermore, the inhibition rate under hydrogen-production conditions (−0.4 V vs SHE) was estimated to be significantly slower for CrHydA1 and DdHydAB than under hydrogen-oxidizing conditions. For CaHydA it is about the same, which was attributed to diffusion control.[20] A model was proposed by Goldet et al.,[20] which explains the catalytic reaction discrimination (faster inhibition under oxidative conditions) by selective reaction of O_2 with H_{ox} and not H_{red}.

With the conclusions drawn from our model calculations we may extend the model of Goldet et al. of the inhibition process by the following proposals. (i) The fact that the inhibition kinetics under oxidative conditions (i.e., electron flow from the H cluster) anticorrelates with reactivity (the faster H_2 production, the slower O_2 inhibition) may also be rationalized with more active enzymes being able to faster supply protons to fully reduce O_2 to water. (ii) One would expect ROS-induced damage to be faster at more negative potentials, because ROS formation is a reductive activation of O_2. This was, however, not observed in experiment by Goldet et al.[20] As explanation the authors point to the selectivity of O_2 for H_{ox} and not H_{red}.[20] From our calculations we conclude that a full reduction of O_2 to water requires electron transfer to the H cluster, otherwise the third and fourth protonation steps become unlikely. For a more reduced H cluster the probability of water formation instead of ROS dissociation is increased. This could be an additional reason for a slower H cluster destruction under more negative electrode potentials.

7. CONCLUSIONS

The optimization of all relevant reaction barriers allowed us to establish a comprehensive kinetic picture of oxygen activation at the H cluster of [FeFe] hydrogenases. Proton transfer to Fe-coordinated reduced O_2 species is fast with low activation barriers. Water formation is preceded by H_2O_2 formation, especially when the proton transfer chain ends with the bridgehead amine group as terminal proton donor of the proton transfer relay. In a more reduced state of the H cluster, proton transfer to the oxygen species coordinated to Fe_d is accelerated. Every intermediately formed Fe-coordinated ROS could dissociate from the H cluster. However, only dissociation reactions of negatively charged ROS are energetically strongly favored for a fully solvated reference state. ROS formation is therefore kinetically controlled by competition with further proton supply that ultimately results in water production. If sufficiently many protons and electrons are available oxygen reduction to water will be feasible. Water formation is always the most exothermic reaction. In a scenario without electron transfer to the H cluster during O_2 activation and with electron transfer coupled to the second proton transfer to the H cluster, two major branching points were identified. In the hydrogen peroxide-bound intermediate, the O−O bond could be cleaved to form water and an iron-oxo species before H_2O_2 dissociates. This reaction has barriers of about +10 kcal/mol, and hence is feasible but not fast in comparison to proton transfers. At the second branching point, CO_2 formation, which has a barrier of +12.2 kcal/mol (oxidized H cluster) or +6.1 kcal/mol (one-electron reduced H cluster), could occur if an iron-oxo species is formed. Additional proton supply leads to hydroxo-ligand formation followed by water formation. If all proton transfer steps to the H cluster are sufficiently fast and coupled to electron transfer, oxygen reduction to water without harmful side reactions will be possible.

■ ASSOCIATED CONTENT

Supporting Information

Additional computational details, energies, and coordinates. This material is available free of charge via the Internet at http://pubs.acs.org.

■ AUTHOR INFORMATION

Corresponding Author

*E-mail: markus.reiher@phys.chem.ethz.ch. Phone: +41 44 633 43 08. Fax: +41 44 633 15 94.

Notes

The authors declare no competing financial interest.

■ ACKNOWLEDGMENTS

This work has been financially supported by the Schweizerischer Nationalfonds (Project No. 200021L_138536) and ETH Zurich (Grant No. ETH-08 11-2).

■ REFERENCES

(1) Lubitz, W.; Ogata, H.; Rüdiger, O.; Reijerse, E. *Chem. Rev.* **2014**, *114*, 4081−4148.
(2) Zirngibl, C.; Hedderich, R.; Thauer, R. K. *FEBS Lett.* **1990**, *261*, 112−116.
(3) Vignais, P. M.; Billoud, B. *Chem. Rev.* **2007**, *107*, 4206−4272.
(4) Shima, S.; Thauer, R. K. *Chem. Rec.* **2007**, *7*, 37−46.
(5) Vignais, P. M.; Billoud, B.; Meyer, J. *FEMS Microbiol. Rev.* **2001**, *25*, 455−501.
(6) Adams, M. W. *Biochim. Biophys. Acta* **1990**, *1020*, 115−145.
(7) Vincent, K. A.; Parker, A.; Armstrong, F. A. *Chem. Rev.* **2007**, *107*, 4366−4413.
(8) Levin, D. B.; Pitt, L.; Love, M. *Int. J. Hydrogen Energy* **2004**, *29*, 173−185.
(9) Lubitz, W.; Reijerse, E. J.; Messinger, J. *Energy Environ. Sci.* **2008**, *1*, 15−31.
(10) Friedrich, B.; Fritsch, J.; Lenz, O. *Curr. Opin. Biotechnol.* **2011**, *22*, 358−364.
(11) Erbes, D. L.; King, D.; Gibbs, M. *Plant Physiol.* **1979**, *63*, 1138−1142.
(12) Vincent, K. A.; Cracknell, J.; Lenz, O.; Zebger, I.; Friedrich, B.; Armstrong, F. A. *Proc. Natl. Acad. Sci. U.S.A.* **2005**, *102*, 16951−16954.
(13) Stiebritz, M. T.; Reiher, M. *Chem. Sci.* **2012**, *3*, 1739−1751.
(14) Baffert, C.; Demuez, M.; Cournac, L.; Burlat, B.; Guigliarelli, B.; Bertrand, P.; Girbal, L.; Léger, C. *Angew. Chem., Int. Ed.* **2008**, *47*, 2052−2054.
(15) Stripp, S. T.; Goldet, G.; Brandmayr, C.; Sanganas, O.; Vincent, K. A.; Haumann, M.; Armstrong, F. A.; Happe, T. *Proc. Natl. Acad. Sci. U.S.A.* **2009**, *106*, 17331−17336.

(16) Stiebritz, M. T.; Reiher, M. *Inorg. Chem.* **2009**, *48*, 7127−7140. [Erratum: *ibid.*, 2010, *49*, 8645;. Corrigendum: *ibid.*, 2014, *53*, 9981].
(17) Peters, J. W.; Lanzilotta, W. N.; Lemon, B. J.; Seefeldt, L. C. *Science* **1998**, *282*, 1853−1858.
(18) Nicolet, Y.; Piras, C.; Legrand, P.; Hatchikian, C. E.; Fontecilla-Camps, J. C. *Structure* **1999**, *7*, 13−23.
(19) Lemon, B. J.; Peters, J. W. *Biochemistry* **1999**, *38*, 12969−12973.
(20) Goldet, G.; Brandmayr, C.; Stripp, S. T.; Happe, T.; Cavazza, C.; Fontecilla-Camps, J. C.; Armstrong, F. A. *J. Am. Chem. Soc.* **2009**, *131*, 14979−14989.
(21) Kubas, A.; De Sancho, D.; Best, R. B.; Blumberger, J. *Angew. Chem., Int. Ed.* **2014**, *126*, 4165−4168.
(22) Dogaru, D.; Motiu, S.; Gogonea, V. *Int. J. Quantum Chem.* **2009**, *109*, 876−889.
(23) Lambertz, C.; Leidel, N.; Havelius, K. G. V.; Noth, J.; Chernev, P.; Winkler, M.; Happe, T.; Haumann, M. *J. Biol. Chem.* **2011**, *286*, 40614−40623.
(24) Bruska, M. K.; Stiebritz, M. T.; Reiher, M. *J. Am. Chem. Soc.* **2011**, *133*, 20588−20603.
(25) Hong, G.; Pachter, R. *ACS Chem. Biol.* **2012**, *7*, 1268−1275.
(26) Stiebritz, M. T.; Finkelmann, A. R.; Reiher, M. *Eur. J. Inorg. Chem.* **2011**, *2011*, 1163−1171.
(27) Bernhard, M.; Buhrke, T.; Bleijlevens, B.; De Lacey, A. L.; Fernandez, V. M.; Albracht, S. P. J.; Friedrich, B. *J. Biol. Chem.* **2001**, *276*, 15592−15597.
(28) Montet, Y.; Amara, P.; Volbeda, A.; Vernede, X.; Hatchikian, E. C.; Field, M. J.; Frey, M.; Fontecilla-Camps, J. C. *Nat. Struct. Biol.* **1997**, *4*, 523−527.
(29) Volbeda, A.; Montet, Y.; Vernède, X.; Hatchikian, E.; Fontecilla-Camps, J. C. *Int. J. Hydrogen Energy* **2002**, *27*, 1449−1461.
(30) Buhrke, T.; Lenz, O.; Krauss, N.; Friedrich, B. *J. Biol. Chem.* **2005**, *280*, 23791−23796.
(31) Tosatto, S. C.; Toppo, S.; Carbonera, D.; Giacometti, G. M.; Costantini, P. *Int. J. Hydrogen Energy* **2008**, *33*, 570−578.
(32) Leroux, F.; Dementin, S.; Burlat, B.; Cournac, L.; Volbeda, A.; Champ, S.; Martin, L.; Guigliarelli, B.; Bertrand, P.; Fontecilla-Camps, J.; Rousset, M.; Léger, C. *Proc. Natl. Acad. Sci. U.S.A.* **2008**, *105*, 11188−11193.
(33) Dementin, S.; Leroux, F.; Cournac, L.; de Lacey, A. L.; Volbeda, A.; Léger, C.; Burlat, B.; Martinez, N.; Champ, S.; Martin, L.; Sanganas, O.; Haumann, M.; Fernández, V. M.; Guigliarelli, B.; Fontecilla-Camps, J. C.; Rousset, M. *J. Am. Chem. Soc.* **2009**, *131*, 10156−10164.
(34) Liebgott, P.-P.; Leroux, F.; Burlat, B.; Dementin, S.; Baffert, C.; Lautier, T.; Fourmond, V.; Ceccaldi, P.; Cavazza, C.; Meynial-Salles, I.; Soucaille, P.; Fontecilla-Camps, J. C.; Guigliarelli, B.; Bertrand, P.; Rousset, M.; Léger, C. *Nat. Chem. Biol.* **2010**, *6*, 63−70.
(35) Cohen, J.; Kim, K.; King, P.; Seibert, M.; Schulten, K. *Structure* **2005**, *13*, 1321−1329.
(36) Wang, P.-h.; Best, R. B.; Blumberger, J. *Phys. Chem. Chem. Phys.* **2011**, *13*, 7708−7719.
(37) Wang, P.-h.; Best, R. B.; Blumberger, J. *J. Am. Chem. Soc.* **2011**, *133*, 3548−3556.
(38) Wang, P.-h.; Blumberger, J. *Proc. Natl. Acad. Sci. U.S.A.* **2012**, *109*, 6399−6404.
(39) Bingham, A. S.; Smith, P. R.; Swartz, J. R. *Int. J. Hydrogen Energy* **2012**, *37*, 2965−2976.
(40) Ludwig, M.; Cracknell, J. A.; Vincent, K. A.; Armstrong, F. A.; Lenz, O. *J. Biol. Chem.* **2009**, *284*, 465−477.
(41) Cracknell, J. A.; Vincent, K. A.; Ludwig, M.; Lenz, O.; Friedrich, B.; Armstrong, F. A. *J. Am. Chem. Soc.* **2008**, *130*, 424−425.
(42) Fritsch, J.; Löscher, S.; Sanganas, O.; Siebert, E.; Zebger, I.; Stein, M.; Ludwig, M.; Lacey, A. L. D.; Dau, H.; Friedrich, B.; Lenz, O.; Haumann, M. *Biochemistry* **2011**, *50*, 5858−5869.
(43) Fritsch, J.; Scheerer, P.; Frielingsdorf, S.; Kroschinsky, S.; Friedrich, B.; Lenz, O.; Spahn, C. M. T. *Nature* **2011**, *479*, 249−252.
(44) Shomura, Y.; Yoon, K. S.; Nishihara, H.; Higuchi, Y. *Nature* **2011**, *479*, 253−257.
(45) Goris, T.; Wait, A. F.; Saggu, M.; Fritsch, J.; Heidary, N.; Stein, M.; Zebger, I.; Lendzian, F.; Armstrong, F. A.; Friedrich, B.; Lenz, O. *Nat. Chem. Biol.* **2011**, *7*, 310−318.
(46) Pandelia, M.-E.; Nitschke, W.; Infossi, P.; Giudici-Orticoni, M.-T.; Bill, E.; Lubitz, W. *Proc. Natl. Acad. Sci. U.S.A.* **2011**, *108*, 6097−6102.
(47) Cracknell, J. A.; Wait, A. F.; Lenz, O.; Friedrich, B.; Armstrong, F. A. *Proc. Natl. Acad. Sci. U.S.A.* **2009**, *106*, 20681−20686.
(48) Liu, Z.-P.; Hu, P. *J. Am. Chem. Soc.* **2002**, *124*, 5175−5182.
(49) Patil, D. S.; Moura, J. J.; He, S. H.; Teixeira, M.; Prickril, B. C.; DerVartanian, D. V.; Peck, H. D.; LeGall, J.; Huynh, B. H. *J. Biol. Chem.* **1988**, *263*, 18732−18738.
(50) Pierik, A. J.; Hagen, W. R.; Redeker, J. S.; Wolbert, R. B. G.; Boersma, M.; Verhagen, M. F. J. M.; Grande, H. J.; Veeger, C.; Mutsaers, P. H. A.; Sands, R. H.; Dunham, W. R. *Eur. J. Biochem.* **1992**, *209*, 63−72.
(51) Pereira, A. S.; Tavares, P.; Moura, I.; Moura, J. J. G.; Huynh, B. H. *J. Am. Chem. Soc.* **2001**, *123*, 2771−2782.
(52) Cao, Z.; Hall, M. B. *J. Am. Chem. Soc.* **2001**, *123*, 3734−3742.
(53) Silakov, A.; Reijerse, E. J.; Albracht, S. P. J.; Hatchikian, E. C.; Lubitz, W. *J. Am. Chem. Soc.* **2007**, *129*, 11447−11458.
(54) Bennett, B.; Lemon, B. J.; Peters, J. W. *Biochem.* **2000**, *39*, 7455−7460.
(55) Roseboom, W.; Lacey, A.; Fernandez, V. M.; Hatchikian, E. C.; Albracht, S. P. J. *J. Biol. Inorg. Chem.* **2006**, *11*, 102−118.
(56) Albracht, S. P. J.; Roseboom, W.; Hatchikian, E. C. *J. Biol. Inorg. Chem.* **2006**, *11*, 88−101.
(57) van Dijk, C.; van Berkel-Arts, A.; Veeger, C. *FEBS Lett.* **1983**, *156*, 340−344.
(58) Nicolet, Y.; de Lacey, A. L.; Vernède, X.; Fernandez, V. M.; Hatchikian, E. C.; Fontecilla-Camps, J. C. *J. Am. Chem. Soc.* **2001**, *123*, 1596−1601.
(59) Hong, G.; Cornish, A.; Hegg, E.; Pachter, R. *Biochim. Biophys. Acta,-Bioenerg.* **2011**, *1807*, 510−517.
(60) Long, H.; King, P. W.; Chang, C. H. *J. Phys. Chem. B* **2014**, *118*, 890−900.
(61) Berggren, G.; Adamska, A.; Lambertz, C.; Simmons, T. R.; Esselborn, J.; Atta, M.; Gambarelli, S.; Mouseca, J.-M.; Reijerse, E.; Lubitz, W.; Happe, T.; Artero, V.; Fontecave, M. *Nature* **2013**, *499*, 66−69.
(62) Pandey, A. S.; Harris, T. V.; Giles, L. J.; Peters, J. W.; Szilagyi, R. K. *J. Am. Chem. Soc.* **2008**, *130*, 4533−4540.
(63) Ahlrichs, R.; Bär, M.; Häser, M.; Horn, H.; Kölmel, C. *Chem. Phys. Lett.* **1989**, *162*, 165−169.
(64) *TURBOMOLE V6.3 2011, a development of University of Karlsruhe and Forschungszentrum Karlsruhe GmbH, 1989−2007, TURBOMOLE GmbH, since 2007; available from* http://www.turbomole.com.
(65) Perdew, J. P. *Phys. Rev. B* **1986**, *33*, 8822−8824.
(66) Becke, A. D. *Phys. Rev. A* **1988**, *38*, 3098−3010.
(67) Grimme, S.; Antony, J.; Ehrlich, S.; Krieg, H. *J. Chem. Phys.* **2010**, *132*, 154104.
(68) Klamt, A.; Schüürmann, G. *J. Chem. Soc., Perkin Trans. 2* **1993**, 799−805.
(69) Sillanpää, A. J.; Aksela, R.; Laasonen, K. *Phys. Chem. Chem. Phys.* **2003**, *5*, 3382−3393.
(70) Weigend, F.; Ahlrichs, R. *Phys. Chem. Chem. Phys.* **2005**, *7*, 3297−3305.
(71) Eichkorn, K.; Weigend, F.; Treutler, O.; Ahlrichs, R. *Theor. Chem. Acc.* **1997**, *97*, 119−124.
(72) Noodleman, L. *J. Chem. Phys.* **1981**, *74*, 5737−5743.
(73) Noodleman, L.; Post, D.; Baerends, E. *Chem. Phys.* **1982**, *64*, 159−166.
(74) Noodleman, L.; Peng, C. Y.; Case, D. A.; Mouesca, J. M. *Coord. Chem. Rev.* **1995**, *144*, 199−244.
(75) Jacob, C. R.; Reiher, M. *Int. J. Quantum Chem.* **2012**, *112*, 3661−3684.
(76) Fiedler, A. T.; Brunold, T. C. *Inorg. Chem.* **2005**, *44*, 9322−9334.
(77) Finkelmann, A. R.; Stiebritz, M. T.; Reiher, M. *Chem. Sci.* **2014**, *5*, 215−221.
(78) Bruschi, M.; Greco, C.; Fantucci, P.; Gioia, L. D. *Inorg. Chem.* **2008**, *47*, 6056−6071.

(79) Bruska, M.; Stiebritz, M. T.; Reiher, M. *Dalton Trans.* **2013**, *42*, 8729−8735.
(80) Herrmann, C.; Reiher, M.; Hess, B. A. *J. Chem. Phys.* **2005**, *122*, 034102.
(81) Mulliken, R. S. *J. Chem. Phys.* **1955**, *23*, 1833−1840.
(82) Reiher, M.; Hess, B. A. *Chem.—Eur. J.* **2002**, *8*, 5332−5339.
(83) Marenich, A. V.; Cramer, C. J.; Truhlar, D. G. *J. Phys. Chem. B* **2009**, *113*, 6378−6396.
(84) Frisch, M. J.; Frisch, M.; Trucks, G. W.; Schlegel, H. B.; Scuseria, G. E.; Robb, M. A.; Cheeseman, J. R.; Scalmani, G.; Barone, V.; Mennucci, B.; Petersson, G. A.; Nakatsuji, H.; Caricato, M.; Li, X.; Hratchian, H. P.; Izmaylov, A. F.; Bloino, J.; Zheng, G.; Sonnenberg, J. L.; Hada, M.; Ehara, M.; Toyota, K.; Fukuda, R.; Hasegawa, J.; Ishida, M.; Nakajima, T.; Honda, Y.; Kitao, O.; Nakai, H.; Vreven, T.; Montgomery Jr., J. A.; Peralta, J. E.; Ogliaro, F.; Bearpark, M.; Heyd, J. J.; Brothers, E.; Kudin, K. N.; Staroverov, V. N.; Kobayashi, R.; Normand, J.; Raghavachari, K.; Rendell, A.; Burant, J. C.; Iyengar, S. S.; Tomasi, J.; Cossi, M.; Rega, N.; Millam, J. M.; Klene, M.; Knox, J. E.; Cross, J. B.; Bakken, V.; Adamo, C.; Jaramillo, J.; Gomperts, R.; Stratmann, R. E.; Yazyev, O.; Austin, A. J.; Cammi, R.; Pomelli, C.; Ochterski, J. W.; Martin, R. L.; Morokuma, K.; Zakrzewski, V. G.; Voth, G. A.; Salvador, P.; Dannenberg, J. J.; Dapprich, S.; Daniels, A. D.; Farkas, O.; Foresman, J. B.; Ortiz, J. V.; Cioslowski, J.; Fox, D. J. *Gaussian 09 Revision D.01;* Gaussian, Inc.: Wallingford, CT, 2009.
(85) Klots, C. E. *J. Phys. Chem.* **1981**, *85*, 3585−3588.
(86) Tawa, G. J.; Topol, I. A.; Burt, S. K.; Caldwell, R. A.; Rashin, A. A. *J. Chem. Phys.* **1998**, *109*, 4852−4863.
(87) Abrahams, S. C.; Kalnajs, J. *Acta Crystallogr.* **1955**, *8*, 503−506.
(88) Dietzel, P. D. C.; Kremer, R. K.; Jansen, M. *J. Am. Chem. Soc.* **2004**, *126*, 4689−4696.
(89) Silaghi-Dumitrescu, R.; Cooper, C. E. *Dalton Trans.* **2005**, 3477−3482.
(90) Abrahams, S. C.; Kalnajs, J. *Acta Crystallogr.* **1954**, *7*, 838−842.
(91) Zheng, J.; Wang, D.; Thiel, W.; Shaik, S. *J. Am. Chem. Soc.* **2006**, *128*, 13204−13215.
(92) Schöneboom, J. C.; Lin, H.; Reuter, N.; Thiel, W.; Cohen, S.; Ogliaro, F.; Shaik, S. *J. Am. Chem. Soc.* **2002**, *124*, 8142−8151.
(93) Rohde, J.-U.; In, J.-H.; Lim, M. H.; Brennessel, W. W.; Bukowski, M. R.; Stubna, A.; Münck, E.; Nam, W.; Que, L. *Science* **2003**, *299*, 1037−1039.
(94) Greco, C.; Bruschi, M.; De Gioia, L.; Ryde, U. *Inorg. Chem.* **2007**, *46*, 5911−5921.
(95) Fan, H.-J.; Hall, M. B. *J. Am. Chem. Soc.* **2001**, *123*, 3828−3829.
(96) Sandala, G. M.; Hopmann, K. H.; Ghosh, A.; Noodleman, L. *J. Chem. Theory Comput.* **2011**, *7*, 3232−3247.
(97) Bergeler, M.; Stiebritz, M. T.; Reiher, M. *ChemPlusChem* **2013**, *78*, 1082−1098.
(98) Becke, A. D. *J. Chem. Phys.* **1993**, *98*, 5648−5652.
(99) Lee, C.; Yang, W.; Parr, R. G. *Phys. Rev. B* **1988**, *37*, 785−789.
(100) Stephens, P. J.; Devlin, F. J.; Chabalowski, C. F.; Frisch, M. J. *J. Phys. Chem.* **1994**, *98*, 11623−11627.
(101) Weymuth, T.; Couzijn, E. P. A.; Chen, P.; Reiher, M. *J. Chem. Theory Comput.* **2014**, *10*, 3092−3103.
(102) Nivière, V.; Fontecave, M. Biological sources of reduced oxygen species. In *Analysis of Free Radicals in Biological Systems;* Favier, A., Cadet, J., Kalyanaraman, B., Fontecave, M., Pierre, J.-L., Eds.; Birkhäuser: Basel, Switzerland, **1995**; pp 11−19.
(103) Sono, M.; Roach, M. P.; Coulter, E. D.; Dawson, J. H. *Chem. Rev.* **1996**, *96*, 2841−2887.
(104) Feig, A. L.; Lippard, S. J. *Chem. Rev.* **1994**, *94*, 759−805.
(105) Costas, M.; Mehn, M. P.; Jensen, M. P.; Que, L. *Chem. Rev.* **2004**, *104*, 939−986.
(106) Kovaleva, E. G.; Lipscomb, J. D. *Nat. Chem. Biol.* **2008**, *4*, 186−193.
(107) Kryatov, S. V.; Rybak-Akimova, E. V.; Schindler, S. *Chem. Rev.* **2005**, *105*, 2175−2226.
(108) McGuire, Jr., R.; Dogutan, D. K.; Teets, T. S.; Suntivich, J.; Shao-Horn, Y.; Nocera, D. G. *Chem. Sci.* **2010**, *1*, 411−414.
(109) Pierre, J.; Fontecave, M. *Biometals* **1999**, *12*, 195−199.